Simulation Model for Hierarchical Self-Assembly of Soft Disklike Particles

Zhan-Wei Li,[†] Zhao-Yan Sun,[‡] and Zhong-Yuan Lu*[,†]

Institute of Theoretical Chemistry, State Key Laboratory of Theoretical and Computational Chemistry, Jilin University, Changchun 130023, China, and State Key Laboratory of Polymer Chemistry and Physics, Changchun Institute of Applied Chemistry, Chinese Academy of Sciences, Changchun 130022, China

Received: October 17, 2009; Revised Manuscript Received: November 27, 2009

We develop a novel mesoscale simulation model in order to study the hierarchical self-assembly of soft disklike particles in dilute solutions. In suitable solvent conditions, the soft anisotropic disklike particles first self-assemble into one-dimensional flexible threads, in accord with experiments. Then, intriguingly, the threads reversibly pack into flexible hexagonal bundles by decreasing the solvent quality. Hierarchical self-assembly of this type may be important to provide a strategy to create bundle structures by bottom-up self-assembly with a single type of *soft and flexible* building block and mimic the bundles commonly found in biological structures.

1. Introduction

Hierarchical self-assembly offers a powerful bottom-up strategy for making functional nanostructures.[1−8] A revolution in novel nanoparticles and colloidal building blocks has brought new excitement to this field.[9] Self-assembly of these new building blocks beyond molecules, which is mainly based on selective control of noncovalent interactions, makes self-assembly reach new heights.[10] Gaining control over noncovalent interactions and making sure the components assemble themselves correctly become an urgent and crucial task for scientists and engineers.[8] Great progress had been made in self-assembly of these new building blocks such as patchy particles,[11,12] Janus particles, colloidal inorganic nanoparticles,[13] polyhedral metal plates,[14] disklike ellipsoidal particles,[15] and so on. Furthermore, Huisman et al. reported phase transition to bundles of flexible supramolecular polymers based on a model of patchy particles,[16] which is inherently via hierarchical self-assembly.

Soft anisotropic particles, such as soft patchy particles,[17] soft disklike micelles,[6,18] and soft disklike molecules,[19] may be used as important building blocks for further hierarchical self-assembly due to their anisotropic interactions and shapes. For example, Wooley and co-workers reported that the anisotropic shape of disklike micelles allows for one-dimensionally preferred growth in experiments.[6] For a better understanding of the hierarchical self-assembly behavior of soft disklike particles, a suitable theoretic model is needed. Nevertheless, to date, there have been no simulation techniques and studies available regarding self-assembly of soft disklike particles into one-dimensional threads or more advanced structures.

Actually, liquid crystal (LC) phase behavior of disklike mesogens and colloidal platelets may serve as a reference for soft disklike particles.[15,20−24] For these mesogens to display LC phases, they must generally be rigid, anisotropic, and above certain concentrations. Although soft disklike particles, such as disklike micelles, are also anisotropic as disklike LC mesogen, they normally exist in dilute solutions and possess a structure with a relatively hard core surrounded by soft coronas. Thus, for such a system, entropy is not dominating as in the LC phase. In addition, we note that, in experiments, the effective interactions between soft disklike particles (consisting of many atoms) may be slightly attractive in the relatively long range arising from hydrophobic, hydrogen bonding, or ionic interactions. The interaction nature between soft disklike particles is different from disklike LC mesogens; therefore, the traditional potential types originating from Lennard-Jones and the purely repulsive potential in dissipative particle dynamics (DPD) may not be suitable to describe the interactions between them. A soft anisotropic potential with relatively strong repulsion at short range and weak attraction at long range is needed to model the interactions between soft disklike particles which consist of many atoms.

Furthermore, hierarchical self-assembly of soft disklike particles involves long time and length scales which are inaccessible in the microscopic simulation techniques. Hence, a larger scale simulation is also very important for studying hierarchical self-assembly of soft disklike particles. In this work, we develop a novel mesoscale simulation model that can reflect the interaction nature between soft anisotropic particles in a simple way, and allows one to study hierarchical self-assembly of *soft anisotropic* particles such as soft disklike micelles and soft disklike molecules.

2. Models and Simulation Details

In the simulations, to reflect the interaction nature between soft disklike particles, we propose an anisotropic potential based on the soft conservative potential in DPD by incorporating the orientation dependence of the particles.[25,26] It is expressed as

$$U_{ij} = \frac{\alpha_{ij}^{R}}{2}(1 - r_{ij})^2 - f^{\nu}\frac{\alpha_{ij}^{A}}{2}(r_{ij} - r_{ij}^{2}) \qquad (1)$$

where

* To whom correspondence should be addressed. E-mail: luzhy@jlu.edu.cn. Phone: 0086 431 88498017. Fax: 0086 431 88498026.
[†] Jilin University.
[‡] Chinese Academy of Sciences.

10.1021/jp909959k
Published on Web 01/19/2010

$$f = \frac{(\mathbf{n}_i \cdot \mathbf{r}_{ij})(\mathbf{n}_j \cdot \mathbf{r}_{ij})}{r_{ij}^2} \quad (2)$$

and $\mathbf{n}_i$ and $\mathbf{n}_j$ are unit vectors assigning the orientation to particle i and j, respectively.[25] The anisotropic factor f is unity if both $\mathbf{n}_i$ and $\mathbf{n}_j$ are parallel to $\mathbf{r}_{ij}$ (the vector connecting the particles i and j). If either $\mathbf{n}_i$ or $\mathbf{n}_j$ or both is perpendicular to $\mathbf{r}_{ij}$, then $f = 0$. If either $\mathbf{n}_i$ or $\mathbf{n}_j$ is antiparallel to $\mathbf{r}_{ij}$, then $f' = -1$ for ν odd and $f' = 1$ for ν even. Here, the magnitude of α_{ij}^{R} controls the strength of repulsion, α_{ij}^{A} controls the strength of attraction, and ν controls the angular width of attraction. Thus, both α_{ij}^{A} and ν control the flexibility of the particle aggregates.

According to eqs 1 and 2, the anisotropic force between two particles is then given by

$$\mathbf{F}_{ij} = \alpha_{ij}^{R}(1 - r_{ij})\frac{\mathbf{r}_{ij}}{r_{ij}} + \alpha_{ij}^{A} f^{\nu}\left(\frac{1}{2} - r_{ij}\right)\frac{\mathbf{r}_{ij}}{r_{ij}} + \frac{\alpha_{ij}^{A}}{2r_{ij}}(r_{ij} - r_{ij}^2)\nu f^{\nu-1}\left[\frac{(\mathbf{n}_i \cdot \mathbf{r}_{ij})\mathbf{n}_j}{r_{ij}} + \frac{(\mathbf{n}_j \cdot \mathbf{r}_{ij})\mathbf{n}_i}{r_{ij}} - 2f\frac{\mathbf{r}_{ij}}{r_{ij}}\right] \quad (3)$$

The translational displacements of the particles follow Newton's equations of motion. The equations of rotational motion can be written as two first-order differential equations[27]

$$\dot{\mathbf{n}}_i = \mathbf{u}_i \quad (4)$$

$$\dot{\mathbf{u}}_i = \mathbf{g}_i^{\perp}/I + \lambda \mathbf{n}_i \quad (5)$$

where I is the moment of inertia. Equation 4 simply defines $\mathbf{u}_i$ as the time derivative of the orientation $\mathbf{n}_i$. Physically, the first term in eq 5 corresponds to the force $\mathbf{g}_i^{\perp}$, the perpendicular component of $\mathbf{g}_i$, responsible for rotation of the particle, where

$$\mathbf{g}_i^{\perp} = \mathbf{g}_i - (\mathbf{g}_i \cdot \mathbf{n}_i)\mathbf{n}_i \quad (6)$$

with

$$\mathbf{g}_i = \frac{\alpha_{ij}^{A}}{2}(r_{ij} - r_{ij}^2)\nu f^{\nu-1}\frac{(\mathbf{n}_j \cdot \mathbf{r}_{ij})\mathbf{r}_{ij}}{r_{ij}^2} \quad (7)$$

The second term in eq 5 corresponds to the force $\lambda \mathbf{n}_i$ along the vector $\mathbf{n}_i$ which constrains the vector length to be a constant of the motion. The quantity λ can be thought of as a Lagrange multiplier. The equations of both translational and rotational motions are integrated via a half-step leapfrog algorithm.[27,28] In the rotational motion, a full step in the integration algorithm is advanced through the equation

$$\mathbf{u}_i\left(t + \frac{1}{2}\delta t\right) = \mathbf{u}_i\left(t - \frac{1}{2}\delta t\right) + \delta t \mathbf{g}_i^{\perp}(t)/I - 2\left[\mathbf{u}_i\left(t - \frac{1}{2}\delta t\right) \cdot \mathbf{n}_i(t)\right]\mathbf{n}_i(t) \quad (8)$$

The step is completed using

$$\mathbf{n}_i(t + \delta t) = \mathbf{n}_i(t) + \delta t \mathbf{u}_i\left(t + \frac{1}{2}\delta t\right) \quad (9)$$

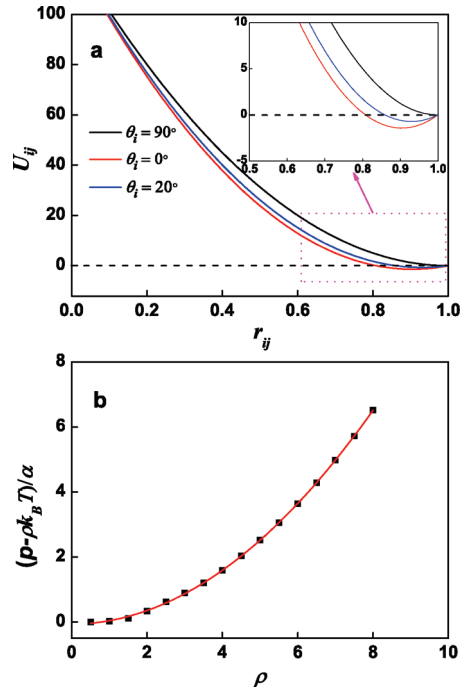

Figure 1. (a) Distance dependence of the anisotropic potential U_{ij} with $\alpha_{ij}^{R} = 250$, $\alpha_{ij}^{A} = 120$, and $\theta_j = 0°$ for three values of θ_i. The weak attraction occurs for $\theta_i = 0°$, and the strength of the attraction decreases for increasing values of θ_i. (b) Excess pressure obtained from simulations. The full curve is a parabola fit. All results are obtained with $\alpha_{ij}^{R} = 250$ and $\alpha_{ij}^{A} = 120$.

The simulations are performed in canonical ensemble. The weak coupling Berendsen thermostat,[28] instead of other typical temperature control schemes in DPD,[29] is used for better control of temperature at the target value. We simulate systems of 2.4×10^4 particles in a $20 \times 20 \times 20$ cubic box with periodic boundary conditions. The number of disklike solute particles is $N_{solute} = 24000 \times \phi$, and the number of solvent particles is $N_{solvent} = 24000 \times (1 - \phi)$ (ϕ is the concentration of the disklike solute particles). The solute−solvent and solvent−solvent interactions follow the first term of eq 1. Here, we use the interaction cutoff radius as the unit of length, $r_c = 1$, the temperature as the unit of energy, $k_B T = 1$, and choose the moment of inertia and the mass of the particle as the units, i.e., $I = m = 1$ for simplicity, thus the time unit $\tau = (m r_c^2/k_B T)^{1/2} = 1$. A time step of $\delta t = 0.002$ is used. All calculations are performed with the in-house developed parallel simulation code.

3. Results and Discussion

For the anisotropic potential in eq 1, if we define that θ_i is the angle between the direction vector $\mathbf{n}_i$ of particle i and the interparticle vector $\mathbf{r}_{ij}$, and θ_j is the angle between the direction vector $\mathbf{n}_j$ of particle j and the interparticle vector $\mathbf{r}_{ij}$, then eq 1 can be rewritten as

$$U_{ij} = \frac{\alpha_{ij}^{R}}{2}(1 - r_{ij})^2 - (\cos\theta_i \cos\theta_j)^{\nu}\frac{\alpha_{ij}^{A}}{2}(r_{ij} - r_{ij}^2) \quad (10)$$

In order to fully understand the anisotropic potential presented in eq 10, we show the dependence of U_{ij} on the interparticle distance for three values of θ_i in Figure 1a, while keeping $\alpha_{ij}^{R} = 250$, $\alpha_{ij}^{A} = 120$, and $\theta_j = 0°$. For $\theta_i = 0°$, there is explicitly weak attraction at long range; as shown in Figure 1a, the

magnitude of the weak attraction is only about $2k_BT$, which is designed to reflect the weak hydrogen bonding or hydrophobic interactions. The strength of the attraction will decrease with increasing θ_i. If θ_i reaches 90°, then $f = 0$ and eq 10 becomes the standard DPD purely repulsive potential $U_{ij} = (\alpha_{ij}/2)(1 - r_{ij})^2$. Therefore, the face-to-face alignment of the disklike particles is energetically favorable. This anisotropic potential is strongly repulsive at short range and weakly attractive at long range, which reflects the interaction nature between soft disklike particles in a simple way.

Groot and Warren[26] presented a successful parabola fitting between the pressure and the particle number density in the standard DPD method: $p = \rho k_BT + \kappa\alpha\rho^2(\rho > 2)$, where κ is the fitting parameter. Subsequently, they mapped the DPD model onto the Flory−Huggins theory and made a link between the DPD repulsion parameters and Flory−Huggins χ parameters. Such mapping implies that the DPD method is suitable to study the mesoscopic systems. We have also studied the dependence of the system pressure on the particle number density to check if our proposed potential ($U_{ij} = (\alpha^R_{ij}/2)(1 - r_{ij})^2 - (\alpha^A_{ij}/2)(r_{ij} - r_{ij}^2)$) can still describe the system on mesoscale. Figure 1b shows the relation between the calculated average pressure and the number density. It is clear that the relation can be fitted well by a parabola function. Thus, our simulation model can still be described well by the Flory−Huggins-type equation of state, which implies that the intrinsic length scale of the newly proposed potential is on mesoscale.

Increasing the repulsion strength α^R_{12} between the disklike particles and the solvent corresponds to varying the solvent condition, which corresponds to cooling or adding another solvent in experiments. Figure 2 shows typical equilibrium packing structures in different solvent conditions. Note that we check the equilibration of our simulations by the snapshots of the systems at different time steps and the time evolution of the order parameters (introduced in the following section) in the simulations. If the structures of the systems at different time steps are very similar and the order parameters reach stable values, the systems are in equilibrium. Moreover, we have also simulated the systems from different initial configurations to check the equilibration. These snapshots in Figure 2 are generated by Qt-based Molecular Graphics Application (QMGA).[30] Each of the simulations starts from the same initially isotropic configuration, as shown in Figure 2a. In a series of simulations, we find that, in slightly good, athermal, and slightly bad solvent conditions, the disklike particles can self-assemble into one-dimensional threads (as shown in Figure 2b), which is in harmony with experiments.[6,19] These one-dimensionally self-assembled threads can reversibly disassemble to the disklike particles again in good solvents (or by heating). Only very weak driving force ($\sim 2k_BT$) is requested for this first order self-assembly.

When the solvent condition becomes bad (i.e., the repulsion strength α^R_{12} is equal to or larger than the critical repulsion parameter for phase separation, which is about $\alpha^R_{12} = 270$ for the concentration of the disklike particles $\phi = 5\%$), phase separation take places, and eventually brings the threads to approach to each other, an intermediate phase characterized by clustering between nearby threads is observed, as shown in Figure 2c. When the solvent quality further decreases, the disklike particles can self-assemble into hexagonal bundle structures (the structure is very similar to the one observed in experiments),[31,32] as can be clearly seen in Figure 2d and e. The bundle thickness is approximately up to 20−30 threads. It should be noted that the bundle is flexible in comparison with

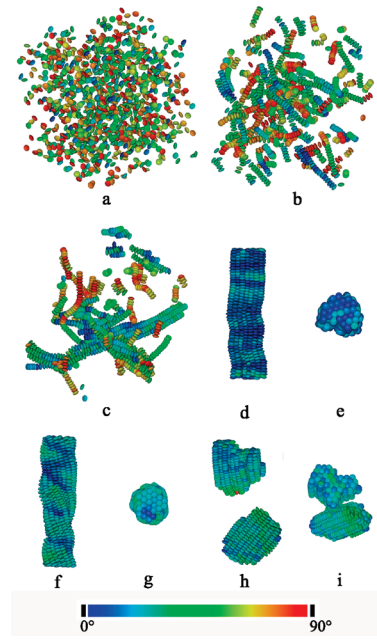

Figure 2. Typical equilibrium packing structures in different solvent conditions. The concentration of disklike particles ϕ is equal to 5%. In these systems, $\alpha^R_{11} = \alpha^R_{22} = 250$, $\nu = 6$, and $\alpha^A_{ij} = 120$, but α^R_{12} is different. (a) Initial configuration. (b) Threads formed in athermal solvent conditions with $\alpha^R_{12} = 250$. (c) Intermediate structure with $\alpha^R_{12} = 300$. (d) Side view of bundle with $\alpha^R_{12} = 330$. (e) Top view of part d. (f) Side view of twisted bundle with $\alpha^R_{12} = 360$. (g) Top view of part f. (h) Side view of broken bundle with $\alpha^R_{12} = 370$. (i) Top view of part h. The color code indicates the orientation according to the palette, and each particle i is colored depending on the absolute value of the angle between the direction vector $\mathbf{n}_i$ of particle i and the director $\mathbf{n}$ (from 0 to 90°). For the sake of clarity, we only show the disklike solute particles in these systems.

that formed by semiflexible filamentous biopolymers,[33−36] since it is hierarchically formed by soft disklike particles in our case. When the solvent condition is even worse, the interfacial tension between the bundle and the solvent becomes larger. This may finally twist the hexagonal bundle, as shown in Figure 2f. The twisted bundle is also hexagonally packed (Figure 2g). When further degrading the solvent quality, the bundle will break into short and thick bundle-like structures (broken bundles) because of the strong interfacial tension. In the present simulations, we may approximately define a criterion for a bundle structure that the average length of each thread should contain at least 25 disklike particles in it. Following this criterion, the broken bundles as shown in Figure 2h and i are actually not well-defined bundles. Therefore, a proper choice of the solvent quality will result in various complex structures originated by hierarchical self-assembly of soft disklike particles. Recent experimental evidence is reported in ref 19. To assess the system size effect, larger boxes with $32 \times 32 \times 32$ (98304 particles) are simulated for selected state points. We also observe the self-assembly structures such as threads, an intermediate phase characterized by the coexistence of threads and bundle-like structures, and a hexagonal bundle for larger systems (as shown in Figure S1 of the Supporting Information). Thus, the finite size effect is negligible in our simulations. We have also examined the influences of the parameter ν and α^A_{ij} on the self-assembled structures of soft disklike particles, shown in the Supporting Information.

In ref 25, they considered a reversibly assembling model exhibiting liquid crystalline phases of linear chains or aggregates as a typical and often examined example for self-organization.

In their model, the monomers interact via a Lennard-Jones-type potential with anisotropic attraction. The self-assembly of soft disklike particles in dilute solutions is different from the phase behavior of reversibly aggregated linear model polymers in ref 25, in which isotropic, nematic, and hexagonal columnar phases are observed. Various self-assembly structures such as threads, hexagonal bundles, twisted bundles, and broken bundles are obtained in our simulations.

The bundle structure may serve as a starting point for further self-assembly to form a physical gel; thus, in order to characterize the inherent structures of the bundles, we calculate four positional correlation functions: $g(r)$, $g_\perp(r_\perp)$, $g_{||}(r_{||})$, and $g_c(r_c)$.[20,21,37−42] The first one is the orientationally averaged pair distribution function $g(r)$, which provides information about the probability of finding a particle at a distance r from the one at the origin

$$g(r) = \frac{1}{4\pi N\rho r^2}\left\langle \sum_i^N \sum_{j\neq i}^N \delta(r - r_{ij})\right\rangle \tag{11}$$

It enables us to distinguish between the ordered and the disordered phases easily. The second distribution function is the perpendicular radial distribution function $g_\perp(r_\perp)$, which gives information about the arrangement of particles in planes perpendicular to the director $\mathbf{n}$.

$$g_\perp(r_\perp) = \frac{1}{2\pi l_t N\rho r_\perp}\left\langle \sum_i^N \sum_{j\neq i}^N \delta(r_\perp - r_{ij,\perp})\right\rangle \tag{12}$$

where $|\mathbf{n}\cdot\mathbf{r}_{ij}| < l_t/2$, $l_t = 1$ is the slice thickness of the particles considered, and $r_{ij,\perp} = (|r_{ij}|^2 - |\mathbf{n}\cdot\mathbf{r}_{ij}|^2)^{1/2}$. We have also calculated the distribution function parallel to the director $g_{||}(r_{||})$ which is sensitive to the arrangement of the disklike particles in layers.

$$g_{||}(r_{||}) = \frac{1}{l_x l_y N\rho}\left\langle \sum_i^N \sum_{j\neq i}^N \delta(r_{||} - \mathbf{n}\cdot\mathbf{r}_{ij})\right\rangle \tag{13}$$

where l_x and l_y are the box dimensions along the X and Y axes, respectively. The last distribution function $g_c(r_c)$ is sensitive to the regular stacking of particles in columns. It is defined as

$$g_c(r_c) = \frac{1}{\pi d^2 N\rho}\left\langle \sum_i^N \sum_{j\neq i}^N \Delta_{ij}\delta(r_c - \mathbf{n}_i\cdot\mathbf{r}_{ij})\right\rangle \tag{14}$$

and it gives the probability of finding a particle j in a cylinder of radius d, with the cylinder axis parallel to the orientation vector $\mathbf{n}_i$ of the particle i at the origin and at resolved distance r_c.[39] Here, d is approximate to $D/2$ (D is the diameter of the disklike particle, which can be estimated through $g(r)$ and $g_\perp(r_\perp)$). The quantity Δ_{ij} makes sure that only the particles belonging to the cylinder are counted. Δ_{ij} is equal to unity if $|\mathbf{n}_i\cdot\mathbf{r}_{ij}|^2 + d^2 > |\mathbf{r}_{ij}|^2$, and zero otherwise; these are convenient for evaluation by computer simulation.[21] For all of these distribution functions, δ is the Dirac delta function, and a histogram with width 0.01 is constructed of all pair separations falling within such a range.

The knowledge of the director orientation $\mathbf{n}$ is required to calculate the radial distribution functions $g_\perp(r_\perp)$ and $g_{||}(r_{||})$. Here, $\mathbf{n}$ is employed to represent the direction for orientational order of the bundle structure, defined to be the average orientation of the disklike particles as in refs 21 and 40. However, the director is not known *a priori* in the computer simulations. Actually, the director fluctuates during the evolution of the system. The orientation of the director for a given configuration can be calculated from a second rank tensor[20,21,37−42]

$$\Omega_{\alpha\beta} = \frac{1}{N}\sum_{i=1}^N \frac{1}{2}(3u_\alpha^i u_\beta^i - \delta_{\alpha\beta}) \tag{15}$$

where $\alpha, \beta = x, y, z$ and u_α^i is the direction cosine of the unit vector describing the orientation of particle i. The Ω tensor is calculated per 7×10^4 time steps and accumulated for 30 consecutive time steps, then averaged and diagonalized. The eigenvectors of the diagonalized Ω tensor are used, and the one associated with the largest eigenvalue is identified as the director. The frequency of eigenvector determination depends on the frequency of sampling of the structural properties.

The radial distribution functions are presented in Figure 3 for the bundle structure shown in Figure 2d and e. Typically, a doublet in the pair distribution functions $g(r)$ and $g_\perp(r_\perp)$ can be taken as the signature of a hexagonal arrangement of the particles.[21] As demonstrated in Figure 3a and b, a doublet between 1.3 and 2.0 appears, which is clear evidence for the hexagonally packed bundle structure. The perpendicular radial distribution function $g_\perp(r_\perp)$ possesses a large peak around $r = 0$, which is attributed to the packing of the particles in the same thread.[38] Moreover, we can approximately estimate the aspect ratio (L/D) of the disklike particles in this system using the pair distribution functions $g(r)$ and $g_\perp(r_\perp)$.[37] The first peak located at 0.45 as shown in Figure 3a is due to the face-to-face packing of the disklike particles along the director. Thus, the thickness of the disklike particle L is roughly taken as 0.45. Similarly, we can obtain the diameter of the disklike particle D through the second peak (at 0.90) in Figure 3a and through Figure 3b which corresponds to the side-by-side packing configurations of the disklike particles. Thus, the aspect ratio (L/D) of the disklike particle is about 0.50. The peaks in $g_{||}(r_{||})$ are regularly spaced with an average spacing of 0.5, which indicates that the bundle is a weakly layered structure with strongly correlated stacking of particles in threads.[21] Indeed, $g_c(r_c)$ is sensitive to the positional correlations of particles that belong to the same thread. The number of oscillations in $g_c(r_c)$ can be considered as a rough measure of the number of particles in a thread. As shown in Figure 3d, we can estimate that the number of particles in a thread is between 40 and 75.[20]

To detect orientational order and hexagonal order of the bundle structures, we also calculate the orientation order parameter Q and the hexagonal order parameter Ψ_6.[21,37,40] The orientation order parameter Q is expressed as[21,37,40]

$$Q = \frac{2}{(N-1)N}\left\langle \sum_i \sum_{j>i} \frac{1}{2}(3\cos^2\theta_{ij} - 1)\right\rangle \tag{16}$$

Here, θ_{ij} is the angle between $\mathbf{n}_i$ and $\mathbf{n}_j$. Note that $\theta_{ij} = 0$ corresponds to $Q = 1$, whereas a random (isotropic) orientation of $\mathbf{n}_i$ results in $Q = 0$. The hexagonal order parameter Ψ_6 is expressed as[21,37,40]

$$\Psi_6 = \left|\left\langle \frac{1}{N}\sum_j \frac{1}{n_b^j}\sum_{\langle kl\rangle} w_{kl}\exp(6i\theta_{kl})\right\rangle\right| \tag{17}$$

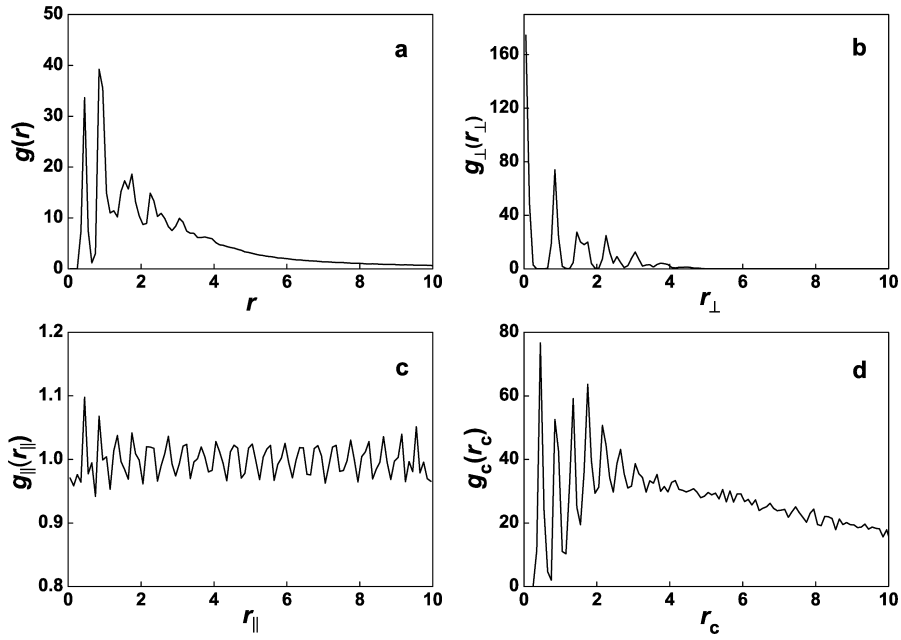

Figure 3. The radial distribution functions: (a) $g(r)$; (b) $g_\perp(r_\perp)$; (c) $g_{\parallel}(r_{\parallel})$; (d) $g_c(r_c)$.

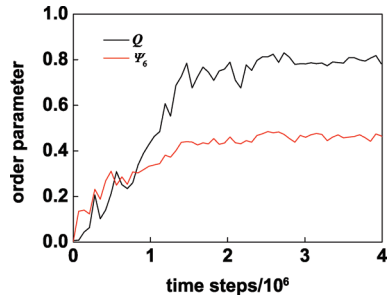

Figure 4. Time evolution of the order parameter: the orientation order parameter Q (black line); the hexagonal order parameter Ψ_6 (red line).

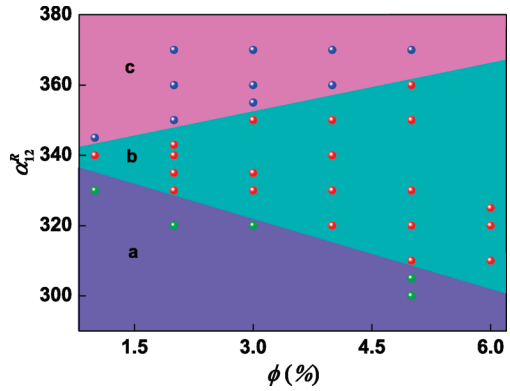

Figure 5. Phase diagram of soft disklike particles. In the simulations, $\alpha^R_{11} = \alpha^R_{22} = 250$, $\nu = 6$, and $\alpha^A_{ij} = 120$. α^R_{12} is the repulsion strength between the disklike particle and the solvent, thus also characterizing the solvent conditions. ϕ is the concentration of disklike particles in the solution. The phase diagram has three regions: (a) intermediate phase; (b) hexagonal bundle; (c) broken bundle. The symbols are the simulation results, and the phase boundaries are drawn manually to guide the eyes.

where n_b^j is the number of pairs of nearest neighbors of the jth particle, $\langle kl \rangle$ implies a sum over all possible pairs of neighbors, and θ_{kl} is the angle between the unit vectors along the projections of the interparticle vectors between particle j and its neighbors k and l onto a plane perpendicular to the director **n** (the director **n** is calculated from eq 15). $w_{kl} = 1$ if r_{jk} and r_{jl} lie within a cylinder of diameter 2 and thickness 1 centered at particle j, and zero otherwise. This range is chosen such that only particles in the first coordination shell contribute to the sum. Ψ_6 takes unity for a phase with a perfect hexagonal order, zero for the isotropic phase, and a value between 0 and 1 for a phase with intermediate hexagonal order. Figure 4 shows the time evolution of Q and Ψ_6 from an initially isotropic configuration in Figure 2a to the bundle structure in Figure 2d and e. As can be seen in Figure 4, for the bundle structure in Figure 2d and e, the orientation order parameter Q is about 0.80 and the hexagonal order parameter Ψ_6 is about 0.46.

We also examine the influence of the solvent quality on the self-assembled bundle structures at different solution concentrations. Figure 5 shows a schematic phase diagram plotted with the concentration ϕ (defined as the ratio between the number of disklike particles and the total number of simulation particles) versus the repulsion strength α^R_{12}. As expected, in relatively bad solvent conditions, we observe the intermediate phase characterized by the coexistence of threads and bundle-like structures. The phase diagram shows that the disklike particles self-assemble into hexagonal bundles in bad solvent conditions, and the bundle phase is much more stable in higher concentrations. The broken bundle phase appears in even worse solvent conditions, and it is easier to be observed in lower concentrations. Therefore, by properly tuning the solvent condition and/or solution concentration, various self-assembly structures such as threads, hexagonal bundles, twisted bundles, and broken bundles can be obtained.

4. Conclusions

In conclusion, we propose an anisotropic potential and simulation technique which is suitable to study the mesoscopic soft discoidal systems efficiently over greater length and time scales. Hierarchical self-assembly of soft disklike particles is successfully investigated with the aid of the simulation model. The soft disklike particles can represent the core−corona micelles with stable structures and the similar kinds of particles. The cooperative driving factors of hierarchical self-assembly of soft disklike particles are the weak noncovalent attraction (only about $2k_BT$) and phase separation. The weak attraction

allows disklike particles to self-assemble into one-dimensional threads. The phase separation does not break the one-dimensional thread structures but brings the threads together to form a hexagonal bundle structure. This new bundle structure can serve as a starting point to form further advanced materials. Therefore, our mesoscopic simulation strategy may represent a useful route to study the hierarchical self-assembly of soft anisotropic systems and design novel and complex structures.

Acknowledgment. This work is supported by the National Science Foundation of China (20774036, 20974040, 50930001) and Graduate Innovation Fund of Jilin University (20091009).

Supporting Information Available: Typical equilibrium structures for the larger systems, and the influence of ν and α_{ij}^{A} on the self-assembled structures of soft disklike particles. This material is available free of charge via the Internet at http://pubs.acs.org.

References and Notes

(1) Jonkheijm, P.; van der Schoot, P.; Schenning, A. P. H. J.; Meijer, E. W. *Science* **2006**, *313*, 80.
(2) Keizer, H. M.; Sijbesma, R. P. *Chem. Soc. Rev.* **2005**, *34*, 226.
(3) Palmer, L. C.; Stupp, S. I. *Acc. Chem. Res.* **2008**, *41*, 1674.
(4) Klein, M. L.; Shinoda, W. *Science* **2008**, *321*, 798.
(5) Srinivas, G.; Discher, D. E.; Klein, M. L. *Nat. Mater.* **2004**, *3*, 638.
(6) Cui, H.; Chen, Z.; Zhong, S.; Wooley, K. L.; Pochan, D. J. *Science* **2007**, *317*, 647.
(7) Glotzer, S. C. *Science* **2004**, *306*, 419.
(8) Service, R. F. *Science* **2005**, *309*, 95.
(9) Glotzer, S. C.; Solomon, M. J. *Nat. Mater.* **2007**, *6*, 557.
(10) Whitesides, G. M.; Boncheva, M. *Proc. Natl. Acad. Sci. U.S.A.* **2002**, *99*, 4769.
(11) Zhang, Z.; Glotzer, S. C. *Nano Lett.* **2004**, *4*, 1407.
(12) Sciortino, F.; Bianchi, E.; Douglas, J. F.; Tartaglia, P. *J. Chem. Phys.* **2007**, *126*, 194903.
(13) Li, M.; Schnablegger, H.; Mann, S. *Nature* **1999**, *402*, 393.
(14) Clark, T. D.; Tien, J.; Duffy, D. C.; Paul, K. E.; Whitesides, G. M. *J. Am. Chem. Soc.* **2001**, *123*, 7677.
(15) Chakrabarti, D.; Wales, D. J. *Phys. Rev. Lett.* **2008**, *100*, 127801.
(16) Huisman, B. A. H.; Bolhuis, P. G.; Fasolino, A. *Phys. Rev. Lett.* **2008**, *100*, 188301.
(17) Srinivas, G.; Pitera, J. W. *Nano Lett.* **2008**, *8*, 611.
(18) Li, Z.; Kesselman, E.; Talmon, Y.; Hillmyer, M. A.; Lodge, T. P. *Science* **2004**, *306*, 98.
(19) Yan, J.-J.; Tang, R.-P.; Zhang, B.; Zhu, X.-Q.; Xi, F.; Li, Z.-C.; Chen, E.-Q. *Macromolecules* **2009**, *42*, 8451.
(20) Veerman, J. A. C.; Frenkel, D. *Phys. Rev. A* **1992**, *45*, 5632.
(21) Zewdie, H. *Phys. Rev. E* **1998**, *57*, 1793.
(22) Care, C. M.; Cleaver, D. J. *Rep. Prog. Phys.* **2005**, *68*, 2665.
(23) van der Kooij, F. M.; Kassapidou, K.; Lekkerkerker, H. N. W. *Nature* **2000**, *406*, 868.
(24) Petukhov, A. V.; van der Beek, D.; Dullens, R. P. A.; Dolbnya, I. P.; Vroege, G. J.; Lekkerkerker, H. N. W. *Phys. Rev. Lett.* **2005**, *95*, 077801.
(25) Fodi, B.; Hentschke, R. *J. Chem. Phys.* **2000**, *112*, 6917.
(26) Groot, R. D.; Warren, P. B. *J. Chem. Phys.* **1997**, *107*, 4423.
(27) Allen, M. P.; Tildesley, D. J. *Computer Simulation of Liquids*; Clarendon Press: Oxford, U.K., 1987.
(28) Berendsen, H. J. C.; Postma, J. P. M.; van Gunsteren, W. F.; DiNola, A.; Haak, J. R. *J. Chem. Phys.* **1984**, *81*, 3684.
(29) Chen, L.-J.; Lu, Z.-Y.; Qian, H.-J.; Li, Z.-S.; Sun, C.-C. *J. Chem. Phys.* **2005**, *122*, 104907.
(30) Gabriel, A. T.; Meyer, T.; Germano, G. *J. Chem. Theory Comput.* **2008**, *4*, 468.
(31) Sakurai, K.; et al. *Langmuir* **2003**, *19*, 8211.
(32) Varghese, S.; Kumar, N. S. S.; Krishna, A.; Rao, D. S. S.; Prasad, S. K.; Das, S. *Adv. Funct. Mater.* **2009**, *19*, 2064.
(33) Claessens, M. M. A. E.; Semmrich, C.; Ramos, L.; Bausch, A. R. *Proc. Natl. Acad. Sci. U.S.A.* **2008**, *105*, 8819.
(34) Daga, R. R.; Lee, K.-G.; Bratman, S.; Salas-Pino, S.; Chang, F. *Nat. Cell Biol.* **2006**, *8*, 1108.
(35) Needleman, D. J.; Ojeda-Lopez, M. A.; Raviv, U.; Miller, H. P.; Wilson, L.; Safinya, C. R. *Proc. Natl. Acad. Sci. U.S.A.* **2004**, *101*, 16099.
(36) Hung, A. M.; Stupp, S. I. *Nano Lett.* **2007**, *7*, 1165.
(37) Li, Z.-W.; Chen, L.-J.; Zhao, Y.; Lu, Z.-Y. *J. Phys. Chem. B* **2008**, *112*, 13842.
(38) Andrienko, D.; Marcon, V.; Kremer, K. *J. Chem. Phys.* **2006**, *125*, 124902.
(39) Cinacchi, G.; Tani, A. *J. Chem. Phys.* **2002**, *117*, 11388.
(40) Zewdie, H. *J. Chem. Phys.* **1998**, *108*, 2117.
(41) Cinacchi, G.; Colle, R.; Tani, A. *J. Phys. Chem. B* **2004**, *108*, 7969.
(42) Cristinziano, P. L.; Lelj, F. *J. Chem. Phys.* **2007**, *127*, 134506.

JP909959K